JMEPEG
https://doi.org/10.1007/s11665-019-03928-0

1059-9495/$19.00

Morphological Evolution of Mg-Al-La-Ca Alloy Induced by a Mechanical Stirring Process

Sérgio Luiz Telles Bartex, Lírio Schaeffer, and Vinicius Karlinski de Barcellos

(Submitted October 11, 2018; in revised form December 6, 2018)

This paper aims to evaluate the morphological evolution of a magnesium-aluminum alloy (Mg-6Al-3La-1Ca) processed by a mechanical stirring process (MSP) with different stirring times. An apparatus for semisolid metal alloy processing was used to melt and obtain rheocast material. Transformation temperatures were determined at a slow cooling rate using computer-aided cooling curve thermal analysis (CA-CCTA) and differential scanning calorimetry (DSC). Isothermal mechanical stirring (605 °C), at 950 rpm, was carried out with a solid fraction of 0.29 and stirring times of 0, 1, 2, 4, 8 and 10 min, followed by fast cooling in water. The results showed that the microstructure after conventional casting (0 min—no stirring) is composed of an α-Mg dendritic matrix, $Al_{11}La_3$, $(Al,Mg)_2Ca$ and Mg_2Ca compounds. With the 1-min stirring time, it was not possible to obtain globular structures. For stirring times longer than 2 min, a primary α-Mg globular morphology was obtained. Microstructures with 2 min of stirring time showed better globularization than those obtained under the other conditions. Morphological changes were observed for $Al_{11}La_3$ and $(Al,Mg)_2Ca$ after the MSP followed by fast cooling.

Keywords magnesium alloys, rheocasting, semisolid, solidification

1. Introduction

As the lightest structural metallic materials, magnesium alloys have exceptional characteristics, including low density, good castability, high specific strength and good recyclability. These great characteristics have resulted in a significant application value in industrial fields, such as aerospace, automobile and telecommunications (Ref 1).

Ferry et al. (Ref 2) studied the influence of both calcium (1.0% Ca) and lanthanum (3.0% La) addition to a magnesium alloy system (Mg-4.0% Al, 0.5% Zn). They proposed the substitution of misch metal elements by specific amounts of lanthanum (La) and calcium (Ca) to increase creep resistance. However, the structure showed a dendritic matrix and very coarse compounds, which decreased the other mechanical properties.

Other researchers (Ref 3-6) have studied similar systems containing Mg, Al, La and Ca, and they used techniques such as x-ray diffraction (XRD) and transmission electron microscopy (TEM). The researchers reported formation of the following phases: α-Mg, β-$Mg_{17}Al_{12}$, $Al_{11}La_3$, $(Mg,Al)_2Ca$ and Mg_2Ca, Al_4Ca.

However, a conventional casting process creates microsegregation and heterogeneity in the metal matrix. A good way to reduce the microstructural heterogeneity is to process magnesium alloys by a mechanical stirring process (MSP). This method consists of applying shear stresses in the magnesium alloy in the semisolid state. The shear stresses may break dendritic structures and create a globular morphology, improving the mechanical properties (Ref 7). There are different ways to obtain a slurry of magnesium alloy: ultrasonic vibration (Ref 8), mechanical stirring (Ref 9), gas bubble stirring (Ref 10) and frequency electromagnetic stirring (Ref 11).

Mechanical stirring combined with rapid quenching is a simple way to process metallic alloys and obtain globular structures. However, many researchers (Ref 5, 8, 9) have worked with medium cooling rates (1-10 °C/s) and low velocities (below 400 rpm).

On the other hand, Chen et al. (Ref 12) studied how the rheological behavior of a AZ91D magnesium alloy slurry changed during stirring. They first observed an apparent viscosity decrease and then increase. Therefore, they concluded that there is an optimum stirring time of approximately 10 min. However, the morphological evolution was not evaluated in that work.

Therefore, in this work, a mechanical stirring process at high speed (950 rpm) was used to break dendritic structures, and the influence of mechanical stirring time on the magnesium alloy Mg-6Al-3La-1Ca morphology was evaluated after rapid quenching (approximately 200 °C/s).

This article is an invited submission to JMEP selected from presentations at the 73rd World Foundry Congress and has been expanded from the original presentation. 73WFC was held in Krakow, Poland, September 23-27, 2018, and was organized by the World Foundry Organization and Polish Foundrymen's Association.

Sérgio Luiz Telles Bartex and **Vinicius Karlinski de Barcellos**, Post-Graduation Program in Mining, Metallurgical and Materials Engineering – PPGE3M – Foundry Laboratory, Engineering School, Federal University of Rio Grande do Sul, Bento Gonçalves Av., 9500, Porto Alegre, RS 91501-970, Brazil; and **Lírio Schaeffer**, Post-Graduation Program in Mining, Metallurgical and Materials Engineering – PPGE3M –Metal Forming Laboratory, Engineering School, Federal University of Rio Grande do Sul, Bento Gonçalves Av., 9500, Porto Alegre, RS 91501-970, Brazil. Contact e-mail: bartex@ufrgs.br.

Published online: 15 February 2019

2. Materials and Methods

The experiments were performed with magnesium alloy ingots with the nominal composition Mg-6Al-3La-1Ca, produced by a Brazilian company, and the chemical composition is presented in Table 1.

A resistance-type electric closed furnace with a protective gas atmosphere (commercial argon gas, 99.9%) was designed to prevent any reaction between oxygen and molten magnesium to avoid ignition (Ref 2). A schematic representation of the assembly used in the experiments is presented in Fig. 1.

To obtain the transformation temperatures, a magnesium alloy ingot of 2 kg was melted inside the furnace at 740 °C. The slow cooling condition was obtained by powering off the furnace when the metal reached the desired temperature. The cooling conditions were as close as possible to thermodynamic equilibrium.

The temperature in the ingots was acquired during solidification by a bank of type K thermocouples (1.6 mm diameter, AISI/SAE 446 chromium-steel) that were accurately positioned with respect to the metal/mold interface. Five thermocouples were used, and they were positioned according to the following distances: 15, 30, 45, 60 and 75 mm away from the base, as indicated in Fig. 1(b). Computer-aided cooling curve thermal analysis (CA-CCTA) and differential scanning calorimetry (DSC) were used to estimate the solidification parameters and determine the cooling rate before ingot solidification. The cooling rate applied in the DSC analysis was 0.04 °C/s.

On the other hand, in the rheocasting experiments, a magnesium alloy ingot of 1 kg was melted inside the furnace at 650 °C, and after melting, the temperature was reduced to 605 °C to obtain a 0.29 solid fraction. At the final temperature, mechanical stirring was applied for different times: 0, 1, 2, 4, 8 and 10 min. After each defined time, a cylindrical sample 70 mm in length and 3 mm in diameter was extracted from the semisolid magnesium slurry by suction and immediately cooled in water at 25 °C (Ref 9). Cross sections of the samples were cut to be analyzed by metallography techniques. Polished specimens were investigated by scanning electron microscopy (SEM) and energy dispersive spectrometry (EDS). After etching with a Nital 3% solution (3 mL HNO3 + 97 mL ethanol), an optical microscope was used for metallographic analysis.

Table 1 Chemical composition of the magnesium alloy employed in this work (wt.%)

Elements								
Mg	**Al**	**Zn**	**Mn**	**Fe**	**Cu**	**Ni**	**Ca**	**La**
Balance	5.9	0.03	0.3	0.0058	0.0024	0.0012	0.988	2.77

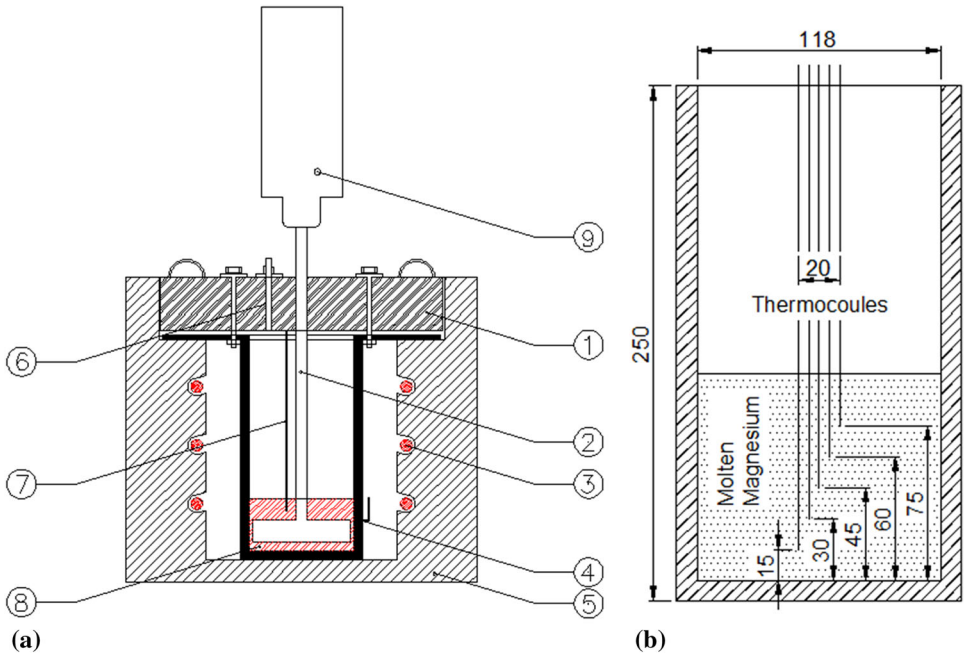

Fig. 1 (a) Schematic representation of the experimental casting equipment: (1) cover, (2) mechanical stirrer, (3) electrical resistances, (4) external thermocouple, (5) thermal insulation, (6) argon inlet, (7) internal thermocouple, (8) magnesium slurry and (9) stirring engine (950 rpm). (b) Thermocouple distribution. Dimensions in mm

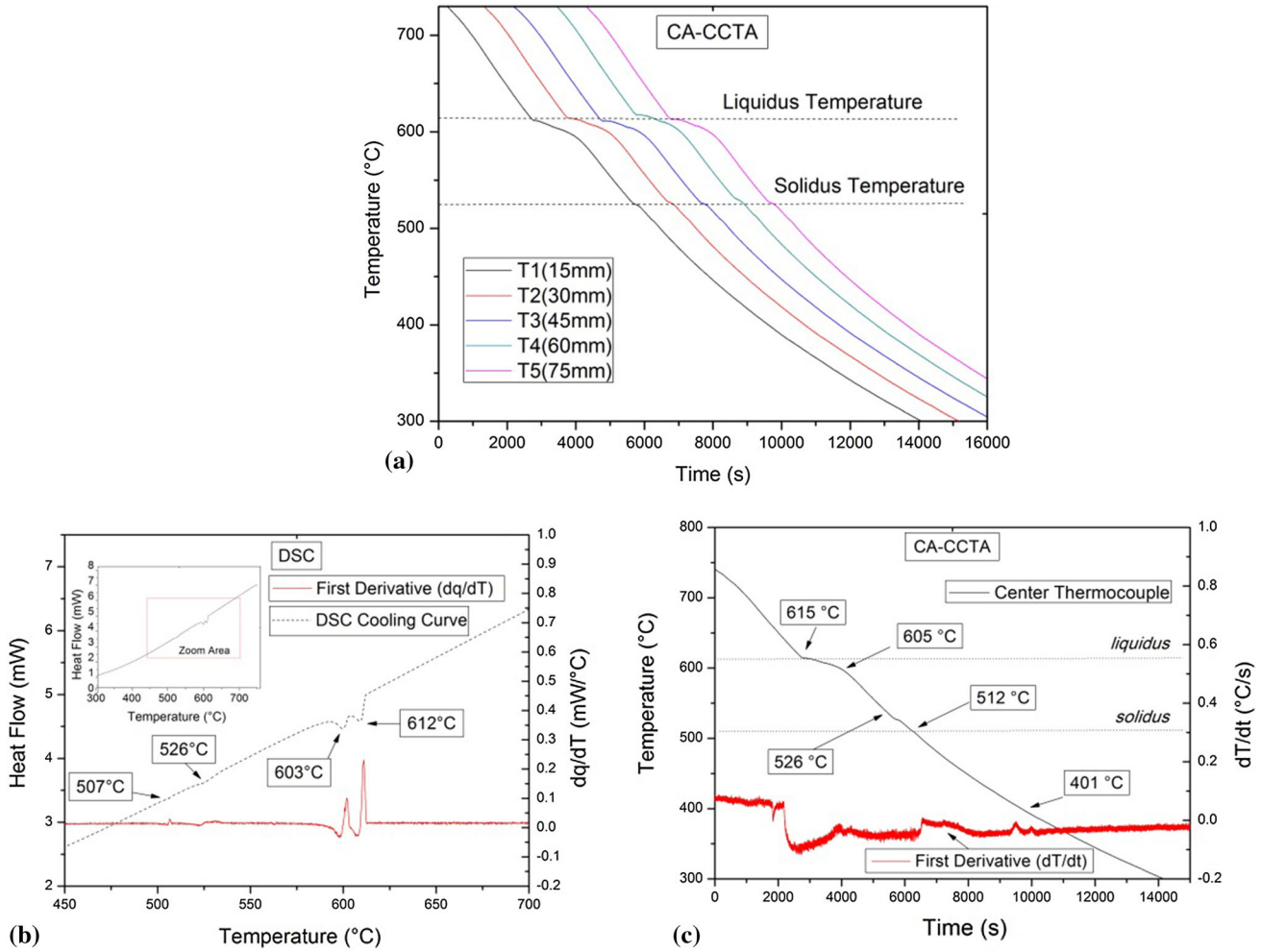

Fig. 2 Cooling curves under slow cooling conditions for all thermocouples. (a) Dashed line shows *liquidus* and *solidus* temperatures determined by thermal analysis (all cooling curves started at the same time, but they are staggered for a better view). (b) DSC results showing the transformation temperatures. (c) CA-CCTA technique applied on a thermocouple 15 mm from the base

Table 2 Main solidification temperatures and phase determination: 614.5 °C—matrix α-Mg; 605.7 °C—acicular phase $Al_{11}La_3$; 526.4 °C—eutectic $(Mg,Al)_2Ca$; 512.4 °C—eutectic Mg_2Ca. 401.0 °C—solid transformation

	Thermocouple position (TP)/temperature ,°C					
Phase transformation	**15 mm**	**30 mm**	**45 mm**	**60 mm**	**75 mm**	**Average**
α-Mg	613.3	614.5	613.0	618.1	614.8	614.5 ± 1.8
$Al_{11}La_3$	602.0	605.0	604.0	609.0	606.0	605.7 ± 2.4
$(Mg,Al)_2Ca$	524.0	527.0	525.0	531.0	524.0	526.4 ± 3.0
Mg_2Ca	512.0	512.0	514.0	514.0	512.0	512.4 ± 1.4
Al-Ca phase	401.0	399.0	400.0	402.0	403.0	401.0 ± 1.6

3. Results and Discussion

3.1 Thermal Analysis Results

Figure 2(a) shows the cooling curve for all thermocouples under cooling conditions as close as possible to thermodynamic equilibrium. The thermal analysis results were similar. Therefore, the cooling rate was calculated as the difference between the initial temperature and the nucleation temperature point (740 and 615 °C, respectively). The average cooling rate was approximately 0.04 °C/s (Ref 10).

In Fig. 2(a), there are two strong changes in the cooling curves: the *liquidus* and *solidus* temperatures. The first occurs

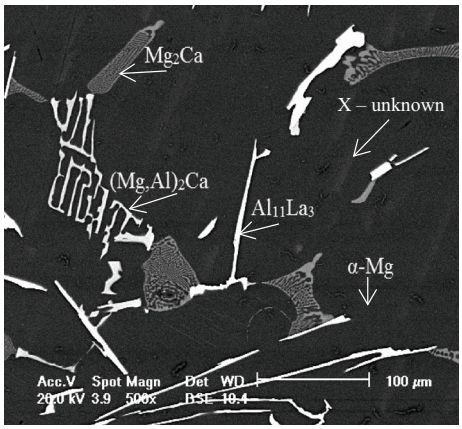

(a)

EDS results (At. %)

Mg	Al	La	Ca	Probable Phase
100	-	-	-	α – Mg
66	27	7	-	$Al_{11}La_3$
67	20	-	13	$(Mg,Al)_2Ca$
72	8	-	20	Mg_2Ca
93	5	-	2	X - unknown

(b)

Fig. 3 (a) Scanning electron microscopy (SEM) image with probable phases and (b) energy dispersive spectroscopy (EDS) results for the 15 mm position, slow cooling rate (no stirring)

at approximately 615 °C and the second occurs at approximately 512 °C, showing a large melting range.

Ferri et al. (Ref 2) studied a similar system, and the *liquidus* temperature was the same. However, the *solidus* temperature was estimated to be 600 °C in their work. Despite this, both techniques (DSC and CA-CCTA) showed that there are other reactions below 600 °C. Ayman et al. (Ref 13) studied a similar system containing lanthanum, and they reported that acicular morphology formation occurred at approximately 599 °C due to the exothermic reaction precipitating the $Al_{11}La_3$ phase. Suzuki et al. (Ref 14) worked with ternary Mg-Al-Ca alloys, and they reported that $(Mg,Al)_2Ca$ and Mg_2Ca transformations occur at approximately 534 and 514 °C, respectively. These results corroborate the thermal analysis performed in the present work.

3.2 Solidification Path of Mg-6Al-3La-1Ca Alloy

Solidification of Mg-6Al-3La-1Ca begins with precipitation of primary α-Mg at 615 °C. At 605 °C, the acicular phase ($Al_{11}La_3$) precipitation begins and is dispersed in the magnesium matrix. The third and fourth reactions that occurred at 526 °C and 512 °C, respectively, are related to both eutectic $(Mg,Al)_2Ca$ and Mg_2Ca phase formation, respectively, and indicate the final solidification. It is possible to observe another reaction at 401 °C that is probably related to the solid-state transformation. Table 2 summarizes the temperatures obtained by each thermocouple after the CA-CCTA analysis. Table 2 summarizes the solidification temperatures by thermocouple.

Figure 3 shows a cross-section SEM image of an ingot that was not stirred and subjected to slow cooling conditions at a region 15 mm away from the base mold (as shown in Fig. 1b).

The microstructures shown in Fig. 3(a) consist of primary magnesium dendrites, formed by α-Mg (dark phase), with different intermetallic phases dispersed along the interdendritic spaces that resulted from solidification of the liquid enriched with alloying elements (Ref 7). Figure 3(b) shows the EDS results. Combining thermal analysis, SEM, EDS and results from the literature (Ref 2-6, 13, 14), the solidification path was probably the following: α-Mg matrix (615 °C), intermetallic precipitation of $Al_{11}La_3$ (605 °C), α-Mg + $(Mg,Al)_2Ca$ (Chinese script-like—534 °C) and α-Mg + Mg_2Ca (networked structure—512 °C).

EDS analysis indicates that phase A contained 100 at.% Mg. However, this result is only qualitative; thus, it could contain other elements dispersed in a solid solution in the matrix (Ref 13). The EDS results were significantly influenced by the matrix due to its relatively large area and depth of analysis compared to the thickness capacity of the probe (Ref 15). This fact could explain why 66% Mg was present in the $Al_{11}La_3$ phase. Despite this, on the very thin structure in Fig. 3(a) indicated as "X-unknown", it can be deduced that the very thin phase containing Al and Ca could be Al_2Ca or Al_4Ca phases. These phases could have been formed through solid transformation caused by the solubility reduction in aluminum and calcium in the α-Mg matrix at low temperature (Ref 3, 16). According to Fig. 2(c), this occurred at approximately 401 °C.

3.3 Morphological Evolution of Mg-6Al-3La-1Ca Alloy

Figure 4 shows the morphological evolution as a function of processing time.

Figure 4 shows the dendritic structure formed by magnesium (α-Mg) and other phases in the interdendritic region (0-min stirring time—as cast) (Ref 2). A 1-min stirring time was not effective in creating globules and could only break the dendritic structures, creating a refinement process.

However, stirring times equal to or greater than 2 min can both break the dendritic structure and create globules in the matrix. These globules were formed by magnesium (α-Mg),

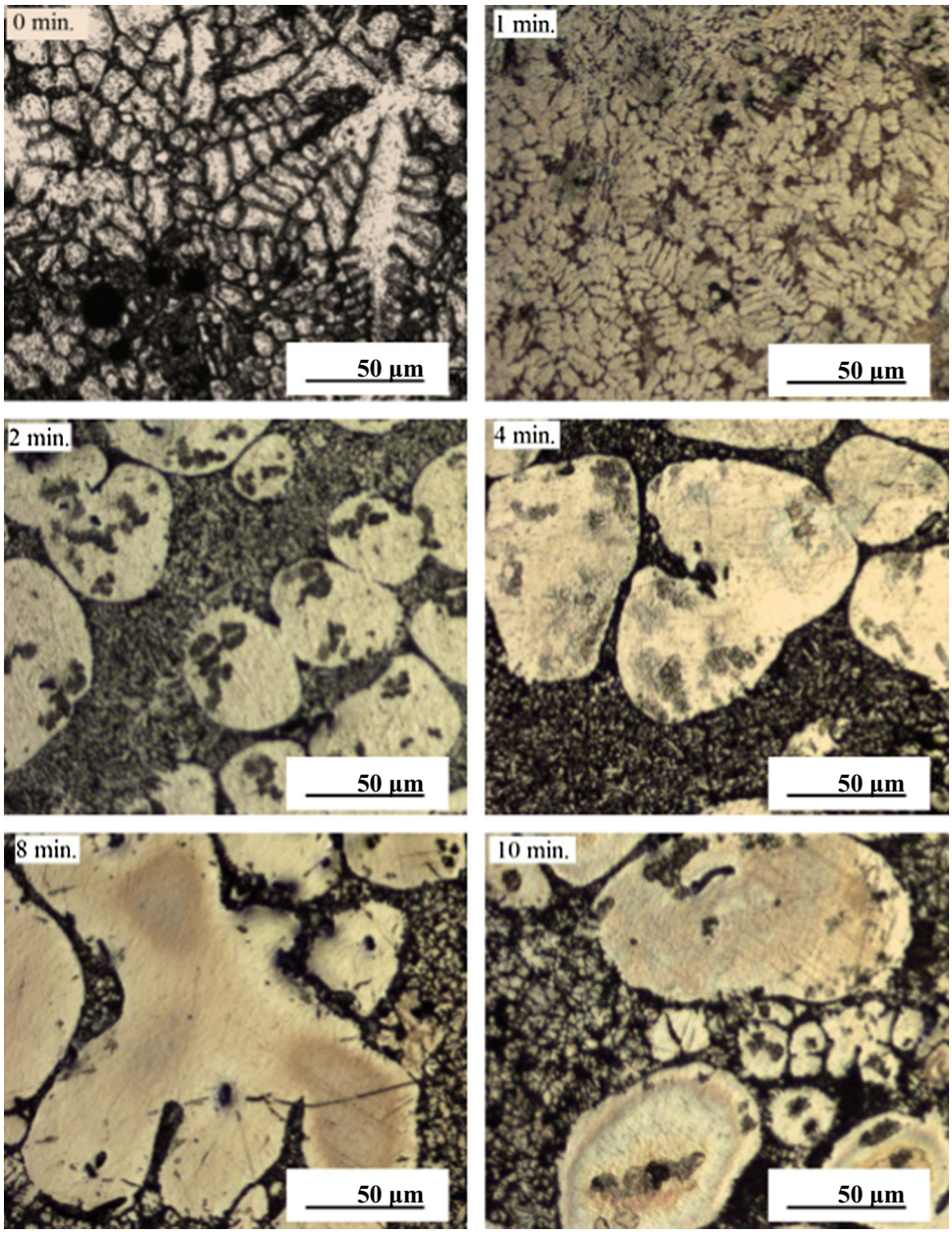

Fig. 4 Morphological evolution as a function of time in Mg-6Al-3La-1Ca alloy processed by MSP. All specimens were stirred at 605 °C and 950 rpm for time t (t = 0, 1, 2, 4, 8, 10 min)

and the interglobular region was formed by the other phases described in Fig. 3.

Additionally, the 2-min stirring time resulted in a more refined globular structure in comparison with that obtained with longer stirring times. At the 4- and 8-min stirring times, the globules started to grow and became coarser. This behavior is in accordance with the Ostwald ripening phenomenon, which is associated with a decrease in the system free energy due to an increase in the area of the globules (Ref 17). Above 2 min of stirring time, all samples presented entrapped liquid inside of globular structures, and as the stirring time increased, the amount of entrapped liquid in the globules also increased. Chen et al. (Ref 18) studied the time influence on the amount of entrapped liquid in magnesium alloy reinforced by SiC. They reported that long processing periods increased the entrapped liquid in globular particles.

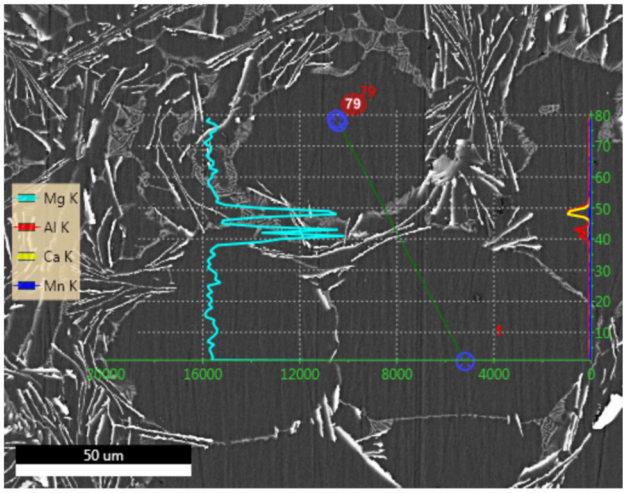

Fig. 5 EDS line scan showing the microsegregation process between globules

With a 10-min stirring time, very coarse structures can be observed in the matrix, and dendritic nucleation began in the remaining liquid, creating small dendritic structures in the interglobular zone in addition to the globules. Figure 5 shows the EDS line scan analysis on globules.

Figure 5 shows the chemical composition distribution from the center of one globule to another globule, and microsegregation can be seen. The primary α-Mg started solidifying, and the Mg content was practically constant inside the globule. At this point, there was approximately a 30% solid fraction, and the remaining liquid was segregated into boundary globules, which contributed to the enrichment of this liquid. Thus, the fast cooling obligated the remaining liquid to start the solidification path, as described in Fig. 3.

Figure 5 also shows that the eutectic $(Mg,Al)_2Ca$ morphology changed from Chinese script-like to a very thin acicular form that was dispersed along the globule boundary. However, the networked structure (Mg_2Ca) had no significant changes after rheocasting.

Figure 6 shows an SEM micrograph and elemental maps obtained by EDS for the sample obtained with 2 min of stirring time.

The elemental map suggests that inside the globules there was a high content of α-Mg (Fig. 6b). As shown in Fig. 6(c) and (d), Al and Ca, respectively, were distributed along the boundary globules and were present as $(Mg,Al)_2Ca$ and Mg_2Ca eutectics. The Al-La distribution indicates intermetallic formation of the $Al_{11}La_3$ acicular morphology. However, it is possible to identify an intermetallic faceted morphology along the metal matrix. The elemental map in Fig. 6(f) shows large manganese content in that compound.

Medina et al. (Ref 19) proposed that 1% Mn addition in a Mg-RE system can create a Mn phase along the matrix. This phase was suspected to be responsible for achieving a good balance of strength and ductility. However, in the present work, Mn was 0.3% in mass, and this element, when combined with lanthanum, created a faceted morphology, as shown in Fig. 7.

4. Conclusion

The *liquidus* and *solidus* temperatures were determined to be 615 and 512 °C, respectively, and the melting range was 103 °C, which is ideal for rheocasting processing.

The solidification path was α-Mg matrix (615 °C), $Al_{11}La_3$ (605°C), α-Mg + $(Mg,Al)_2Ca$ refined eutectic (526 °C) and α-Mg +Mg_2Ca coarse eutectic (512 °C).

The stirring time had a great influence on the morphology of Mg alloy. A 1-min stirring time cannot create globular structures, and conventional dendritic structures of primary α-Mg were found; above 2 min of stirring time, the structures changed from dendritic to globular. As the stirring time further increased, the globule size also increased, and they became coarser due to the Ostwald ripening phenomenon. A 2-min stirring time qualitatively presented better globularization than the other stirring times.

Fast cooling refines the structure and changes the morphology of $(Mg,Al)_2Ca$ from Chinese script-like to an acicular form.

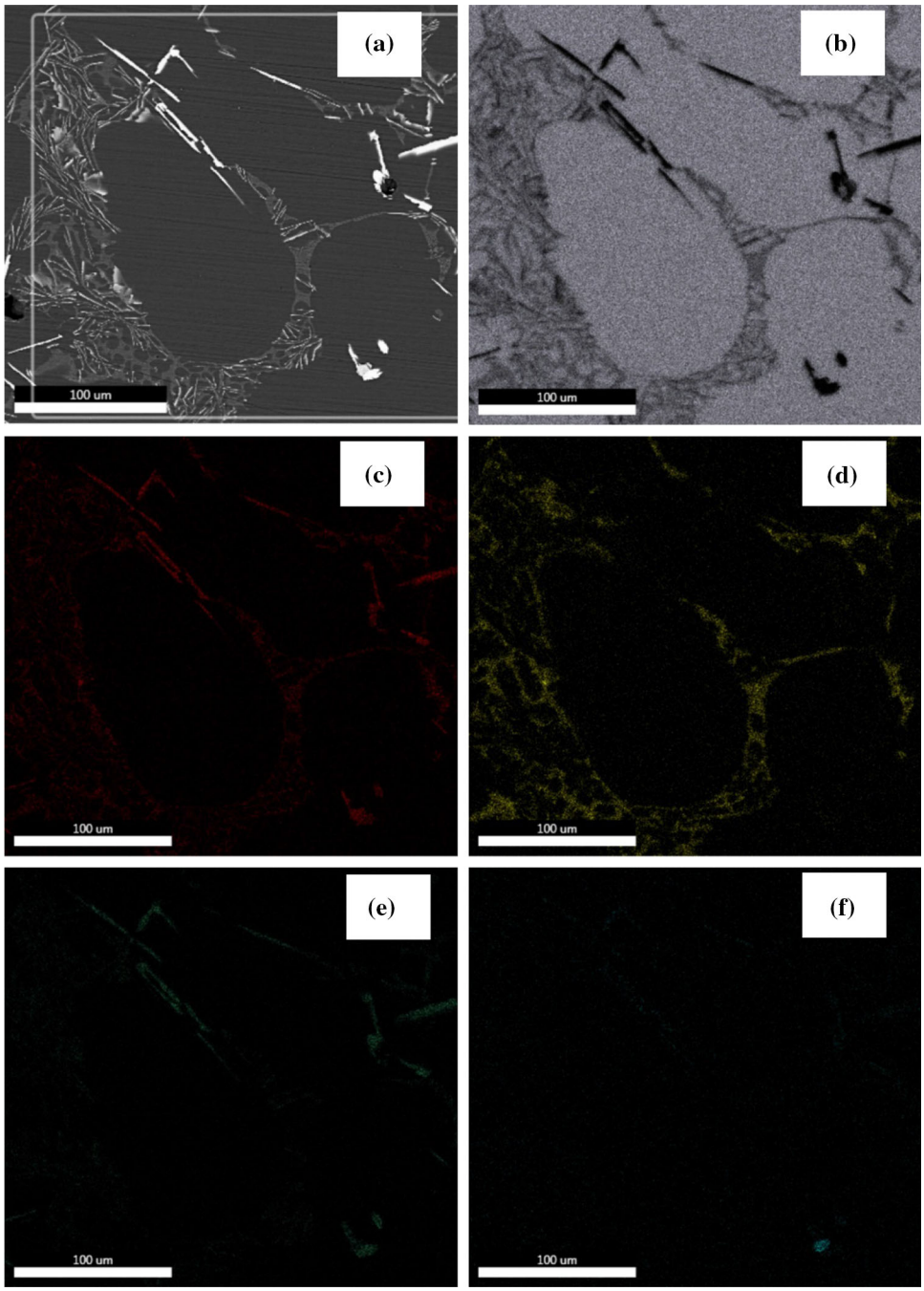

Fig. 6 (a) SEM image and elemental maps for (b) magnesium, (c) aluminum, (d) calcium, (e) lanthanum and (f) manganese in the sample with 2 min of stirring time

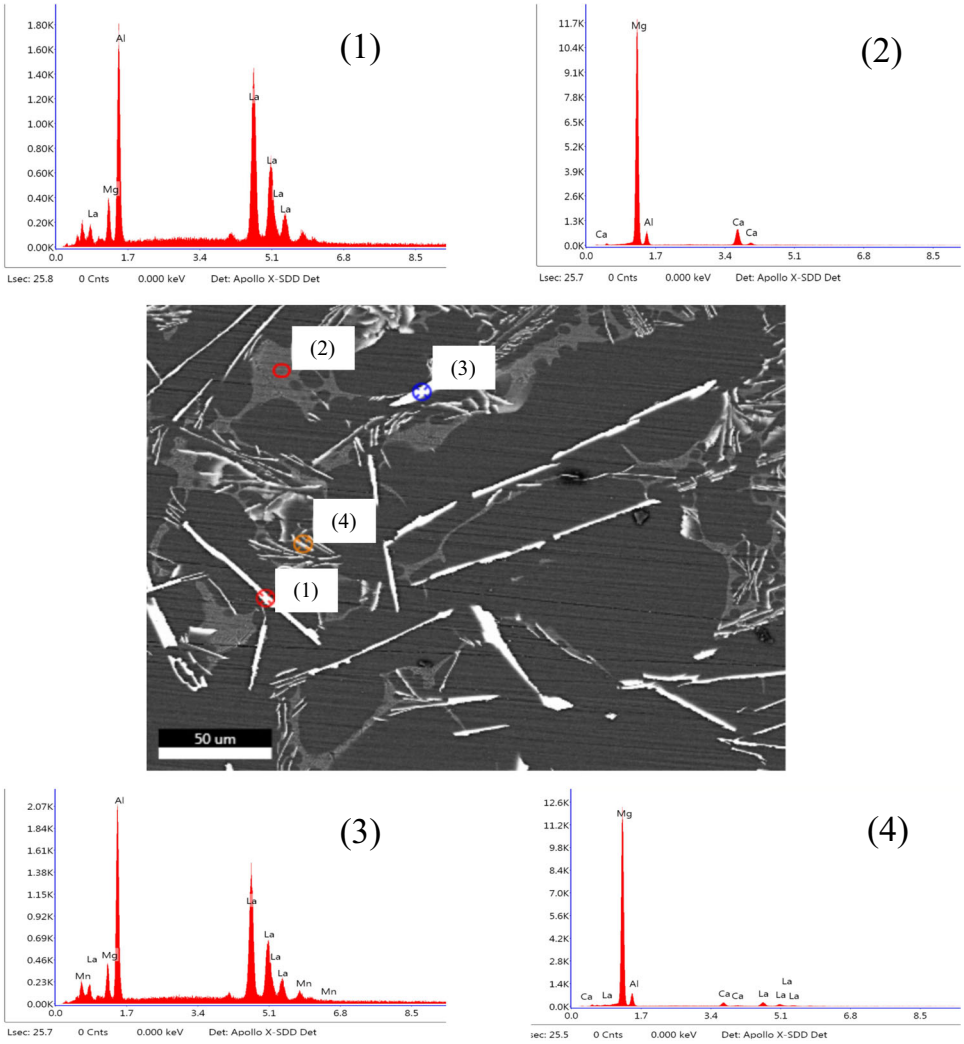

Fig. 7 EDS results for different compounds

Other phases did not change. The manganese content changes the morphology of $Al_{11}La_3$ from acicular to faceted.

Acknowledgments

The authors acknowledge the financial support provided by CNPq and CAPES (Brazilian Research Funding), FAPERGS (The Scientific Research Foundation of the State of Rio Grande do Sul) and the Post-Graduation Program in Mining, Metallurgy and Materials (PPGE3M – UFRGS).

References

1. F. Pan, M. Yang, and X. Chen, Review on Casting Magnesium Alloys: Modification of Commercial Alloys and Development of New Alloys, *J. Mater. Sci. Technol. A*, 2016, **32**, p 1211–1221. https://doi.org/10.1016/j.jmst.2016.07.001
2. T. Ferri, A. Figueiredo, C. Ferreira, W. Hormaza, C. Santos, and J. Spim, Mechanical Properties as a Function of Microstructure in the New Mg-Al-Ca-La Alloy Solidified Under Different Conditions, *Mater. Sci. Eng. A*, 2010, **527**, p 4624–4632. https://doi.org/10.1016/j.msea.2010.03.041
3. X. Fang, S. Lü, L. Zhao, J. Wang, L. Liu, and S. Wu, Microstructure and Mechanical Properties of a Novel Mg-RE-Zn-Y Alloy Fabricated by Rheo-Squeeze Casting, *J. Mater. Des.*, 2016, **94**, p 353–359. https://doi.org/10.1016/j.matdes.2016.01.063
4. W. Zhang, W. Xiao, F. Wang, and C. Ma, Development of Heat Resistant Mg-Zn-Al- Based Magnesium Alloys by Addition of La and Ca: Microstructure and Tensile Properties, *J. Alloys Compd.*, 2016, **684**, p 8–14. https://doi.org/10.1016/j.jallcom.2016.05.137
5. S. Liang, R. Chen, J. Blandin, M. Suery, and E. Han, Thermal Analysis and Solidification Pathways of Mg–Al–Ca System Alloys, *Mater. Sci. Eng. A*, 2008, **480**, p 365–372. https://doi.org/10.1016/j.msea.2007.07.025
6. T. Zhou, Z. Chen, M. Yang, J. Hu, and H. Xia, Investigation on Microstructure Characterization and Property of Rapidly Solidified Mg-Zn-Ca-Ce-La Alloys, *Mater. Charact.*, 2012, **63**, p 77–82. https://doi.org/10.1016/j.matchar.2011.10.004
7. M. Esmaily, N. Mortazavi, J. Svensson, M. Halvarsson, M. Wessén, A. Jarfors, and L. Johansson, Microstructural Characterization of the Mg-Al alloy AM50 Produced by a Newly Developed Rheo-Casting Process, *Mater. Charact.*, 2014, **95**, p 50–64. https://doi.org/10.1016/j.matchar.2014.06.001
8. Z. Zhao, R. Guan, X. Wang, Y. Li, L. Dong, C. Lee, and C. Liu, Microstructure Formation Mechanism and Properties of AZ61 Alloy Processed by Melt Treatment with Vibrating Cooling Slope and Semisolid Rolling, *Met. Mater. Int.*, 2013, **19**, p 1063–1067. https://doi.org/10.1007/s12540-013-5022-2
9. C. Yim and K. Shin, Changes in Microstructure and Hardness of Rheocast AZ91HP Magnesium Alloy with Stirring Conditions, *Mater. Sci. Eng. A*, 2005, **395**, p 226–232. https://doi.org/10.1016/j.msea.2004.12.050

10. R. Canyook, J. Wannasin, S. Wisuthmethangkul, and M. Flemings, Characterization of the Microstructure Evolution of a Semi-Solid Metal Slurry During the Early Stages, *Acta Mater.*, 2012, **60**, p 3501–3510. https://doi.org/10.1016/j.actamat.2012.03.002
11. C. Wang, A. Chen, L. Zhang, W. Liu, G. Wu, and W. Ding, Preparation of an Mg-Gd-Zn Alloy Semisolid Slurry by Low Frequency Electro-Magnetic Stirring, *J. Mater. Des.*, 2015, **84**, p 53–63. https://doi.org/10.1016/j.matdes.2015.06.126
12. H. Chen, J. Chen, and J. Liao, The Influence of Shearing Conditions on the Rheology of Semi-Solid Magnesium Alloy, *Mater. Sci. Eng. A*, 2008, **487**, p 114–119. https://doi.org/10.1016/j.msea.2007.09.072
13. E. Ayman, U. Junko, and K. Katsuyoshi, Application of Rapid Solidification Powder Metallurgy to the Fabrication of High-Strength, High-Ductility Mg-Al-Zn-Ca-La Alloy Through Hot Extrusion, *Acta Mater.*, 2011, **59**, p 273–282. https://doi.org/10.1016/j.actamat.2010.09.031
14. A. Suzuki, N.D. Saddock, J.W. Jones, and T.M. Pollock, Solidification Paths and Eutectic Intermetallic Phases in Mg-Al-Ca Ternary Alloys, *Acta Mater.*, 2005, **53**, p 2823–2834. https://doi.org/10.1016/j.actamat.2005.03.001
15. Y. Du, M. Zheng, X. Qiao, W. Peng, and B. Jiang, Effect of La Addition on the Microstructure and Mechanical Properties of Mg-6 wt.% Zn Alloys, *Mater. Sci. Eng. A*, 2016, **673**, p 47–54. https://doi.org/10.1016/j.msea.2016.07.022
16. B. Kondori and R. Mahmudi, Effect of Ca Additions on the Microstructure and Creep Properties of a Cast Mg-Al-Mn Magnesium Alloy, *Mater. Sci. Eng. A*, 2017, **700**, p 438–447. https://doi.org/10.1016/j.msea.2017.06.007
17. Y. Chen, L. Zhang, W. Liu, G. Wu, and W. Ding, Preparation of Mg-Nd-Zn-(Zr) Alloys Semisolid Slurry by Electromagnetic Stirring, *Mater. Des.*, 2016, **95**, p 398–409. https://doi.org/10.1016/j.matdes.2016.01.131
18. Q. Chen, G. Chen, L. Han, N. Hu, F. Han, Z. Zhao, X. Xia, and Y. Wan, Microstructure Evolution of SiCp/ZM6 (Mg-Nd-Zn) Magnesium Matrix Composite in the Semi-Solid State, *J. Alloys Compd.*, 2016, **656**, p 67–76. https://doi.org/10.1016/j.jallcom.2015.09.135
19. J. Medina, P. Pérez, G. Garcés, and P. Adeva, Effects of Calcium, Manganese and Cerium-Rich Mischmetal Additions on the Mechanical Properties of Extruded Mg-Zn-Y Alloy Reinforced by Quasicrystalline I-Phase, *Mater. Charact.*, 2017, **129**, p 195–206. https://doi.org/10.1016/j.matchar.2017.04.033